ELSEVIER

Journal of Alloys and Compounds 281 (1998) 81–91

Journal of ALLOYS AND COMPOUNDS

Electronic structure and energetics of $LaNi_5$, α-$La_2Ni_{10}H$ and β-$La_2Ni_{10}H_{14}$

H. Nakamura*, D. Nguyen-Manh, D.G. Pettifor

Department of Materials, University of Oxford, Parks Road, Oxford OX1 3PH, UK

Received 30 May 1998; received in revised form 10 August 1998

Abstract

The electronic structure and energetics of $LaNi_5$, its hydrogen solution (α-$La_2Ni_{10}H$) and its hydride (β-$La_2Ni_{10}H_{14}$) were investigated by means of the tight-binding linear muffin-tin orbital method within the atomic sphere approximation (TB-LMTO-ASA). Preferred site occupation of the absorbed hydrogen atoms was investigated in terms of the charge density of the interstitial sites and the total energy, both of which indicate that the 6m site in the *P*6/*mmm* symmetry is the most preferred. A negative heat of formation of $La_2Ni_{10}H_{14}$ was obtained after optimising the kinetic energy of the electrons outside the atomic spheres and the interstitial sphere radii.

Keywords: $LaNi_5$ hydride; Electronic structure; TB-LMTO-ASA; Heat of formation; Preferred site occupancy

1. Introduction

It is almost 30 years since the first hydrogen-absorbing alloy, $LaNi_5$, was discovered in the late 1960s [1]. $LaNi_5$ and its related alloys are still the most important alloys because of their good combination of large hydrogen capacity, moderate stability and excellent electrochemical reactiveness. Both the stability and the hydrogen capacity, which usually display a trade-off relationship (See e.g., Refs. [2–4], need to be controlled in order to design suitable alloys for use in applications. In principle, the stability can be evaluated theoretically, directly from the total energy of the alloys involved in the hydrogenation reaction. In practice, however, no ab-initio theoretical heat of formation for intermetallic-hydrogen systems has been reported yet, due to the complexity of their structures and the vast memory and time required for such a total energy calculation.

In this paper we report the electronic structure and the energetics of $LaNi_5$, its hydrogen solution α-$La_2Ni_{10}H$ and its hydride β-$La_2Ni_{10}H_{14}$, which are calculated with a new linear muffin-tin orbital (LMTO) programme that includes a technique for evaluating interstitial sphere radii [5]. The heat of formation of the hydride is determined by a subtle balance between the total energies of the host alloy and the hydride and is, therefore, easily affected by the accuracy of the calculation. Thus, we first examine the sensitivity of the total energy on the choice of the various parameters appearing in the LMTO calculation. Secondly, we study the site preference of the absorbed hydrogen at low hydrogen concentration (corresponding to the α-phase $La_2Ni_{10}H$) by evaluating the heat of solution for the different sites and comparing them to the local electronic charge densities. Finally, we investigate the electronic structure and the heat of formation of the hydride β-$La_2Ni_{10}H_{14}$, where we predict for the first time a negative heat of formation. We break up the heat of formation into three distinct contributions arising from the electronic structure, the lattice distortion and the volume expansion, respectively.

2. Details of the calculations

2.1. TB-LMTO method

In the present study we calculated the electronic structure self-consistently by using a new TB-LMTO technique, the details of which are described in Ref. [5]. For solving the one-electron Schrödinger equation, we used the scalar-relativistic LMTO in the atomic-sphere-approximation including the combined correction (ASA+CC). Exchange and correlation contributions were included through the local-density-approximation (LDA) using the von Barth–

*Corresponding author.

0925-8388/98/$ – see front matter
PII: S0925-8388(98)00794-4

Hedin formula [6] with the non-local gradient correction due to Langreth, Mehl and Hu [7,8]. In the ASA+CC, the one-electron potential entering the Schrödinger equation is a superposition of overlapping spherical potential wells with positions **R** and radii $s_{\mathbf{R}}$. This approximation leads to a kinetic-energy error proportional to the fourth power of the relative sphere overlap [9]:

$$\omega_{\mathrm{RR}'} \equiv \frac{s_{\mathrm{R}} + s_{\mathrm{R}'}}{|\mathrm{R} - \mathrm{R}'|} - 1 \tag{1}$$

The overlapping of the MT spheres was determined from a full-potential construction [14]. For open structures like intermetallic hydrides, the ASA with only atom-centred spheres would be accompanied by substantial errors, either due to large overlap and misrepresentation of the potential, or due to neglect of the charge in the van der Waals gap. Therefore it is necessary to pack the van der Waals gap with interstitial spheres. The general requirement for choosing the sphere positions and radii of the interstitial spheres is that the superposition of the spherical potentials approximates the full three-dimensional potential [10,11] as accurately as possible, so that the overlap error for the kinetic energy be acceptable. Here we model the full potential by the superposition of neutral-atom potentials, and for simplicity, retain only the Hartree part. The atomic-centred spheres are then determined by tracing the potential along the lines connecting nearest neighbour atoms and finding the saddle-points. For a given atom with position **R**, the distance to the closest saddle-point is taken as the radius of a sphere which usually touches the spheres constructed in the same way about other atoms. The ASA radii are then obtained by inflating these atom-centred non-overlapping spheres until they either fill space or until their overlap reaches a maximum value, which is usually set at 16%. In the latter case, the potential between the atomic potentials must be represented by additional interstitial spheres. The positions of these interstitial spheres are chosen from the non-occupied symmetry positions of the space group. Their radii are normally chosen in such way that the maximum overlap between an atomic and an interstitial sphere is 18% and that between two interstitial spheres is 20%. If these overlap conditions are changed, the total number of the interstitial spheres may vary accordingly. The influence of the overlap conditions on the total energy will be discussed in Section 3.1.1.

It has been realised that the LMTO basis set $|\chi^{\alpha}\rangle$ can be transformed exactly into the orthogonal TB basis set $|\chi^{\alpha}\rangle$ [12]; these transformations are of the form [13],

$$|\chi^{\alpha}\rangle = |\chi^{0}\rangle(1 \pm \alpha S^{\alpha}), \tag{2}$$

where S^{α} is the screened structure matrix and α is a set of the screening constants and is regarded as a diagonal matrix with elements $\alpha_{\mathbf{R}L}$ (**R** and $L \equiv lm$ denote the site and the angular momentum character, respectively). The screened structure matrix S^{α} is given in terms of the canonical structure matrix S^{0} through the following screening transformation or the Dyson equation:

$$S^{\alpha} = S^{0}(1 - \alpha S^{0})^{-1}, \tag{3}$$

where the set of the screening constants $\{\alpha_{\mathbf{R}L}\}$ specifies the representation. In the TB representation, the structure constant matrix S^{α} can be generated in *real space* for each site **R** by inverting the Hermitian matrix $\alpha^{-1} - S^{0}$ for the cluster of 20~50 nearest neighbours **R**′. With the choice $\alpha_{\mathbf{R}L} \equiv \gamma_{\mathbf{R}L}$ from self-consistent LMTO-ASA calculations, the LMTO's become orthonormal with neglect of the small potential parameters of a linear method. The Hamiltonian in the orthonormal representation is then expressed as a power series in the following *two-centre TB Hamiltonian*:

$$h^{\alpha}_{\mathrm{R}L,\mathrm{R}'L'} = (c^{\alpha}_{\mathrm{R}l} - \epsilon_{\nu\mathrm{R}l})\delta_{\mathrm{RR}'}\delta_{LL'} + \sqrt{d^{\alpha}_{\mathrm{R}l}}\, S^{\alpha}_{\mathrm{R}L,\mathrm{R}'L'}\, \sqrt{d^{\alpha}_{\mathrm{R}'l'}} \tag{4}$$

with coefficients proportional to $(\alpha_{\mathbf{R}L} - \gamma_{\mathbf{R}L})$. In Eq. (4), ϵ_{ν} are the positions of the concerned energy windows in which a linear method is expected to yield useful results and c^{α} and d^{α} are the potential parameters derived from the slope and amplitude of the corresponding radial wave function at the sphere boundary. Thus the TB-LMTO approach can be regarded as a link between empirical TB methods and possibly more accurate first principle methods.

The basis set consisted of La 4f, 6s, 5d; Ni 3d, 4s, 4p; H 1s and interstitial sphere 1s LMTOs. In addition, La 6p, H 2p, 3d and interstitial sphere 2p partial waves $\chi_{\mathbf{R}l}(\epsilon, r)$ were taken at the fixed energies $\epsilon_{\nu\mathbf{R}l}$ which are the centres of gravity of the occupied parts of the **R***l* projected bands, and were included only in the tails of the LMTOs mentioned above. This treatment corresponds to Löwdin down-folding, and not only reduces the size of the secular matrix but also serves to avoid distortions of the phase shift of the high partial waves [14]. All **k**-space integrations were performed by the tetrahedron method [15]. In all calculations, self-consistency was achieved with a tolerance in the total energy per unit cell of 10^{-2} mRy.

The heats of formation of hydrogen in solution and the hydride were calculated by subtracting the total energy of the host alloy and the absorbed hydrogen molecule from that of the final state. We used the value of −2.320 Ry for the total energy of the hydrogen molecule which was calculated with the von Barth–Hedin exchange-correlation potential [16]. The heat of formation, ΔH, is a direct determinant of the stability of hydrogen in solution or as the hydride. It is related to the equilibrium hydrogen pressure through the van't Hoff equation:

$$\ln(P/P_0) = \frac{\Delta H}{RT} - \frac{\Delta S}{R}, \tag{5}$$

where P_0 is the standard pressure (=0.1 MPa), ΔS is the entropy change, T is the temperature and R is the gas constant. The entropy change in Eq. (5) is dominated by the entropy loss of the gaseous hydrogen, namely −130.8

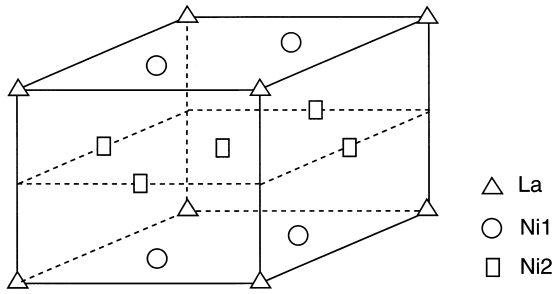

Fig. 1. Crystal structure of $LaNi_5$ ($P6/mmm$).

$J\,K^{-1}mol^{-1}$ H_2 [2]. The other entropy changes arising from lattice vibrations (in particular, the optical phonon branch) and possible different hydrogen configurations are relatively small [17]. In fact, the entropy changes found experimentally are almost the same over a wide range of metal–hydrogen systems [2]. Thus one may concentrate on only the heat of formation in order to understand the relative stability between different structures.

2.2. Crystal structures

$LaNi_5$ has a hexagonal symmetry ($P6/mmm$, structure type $CaCu_5$) as shown in Fig. 1 [1]. The La atom occupies the 1a (0, 0, 0) site and the two nonequivalent Ni atoms occupy the 2c (1/3, 2/3, 0) and the 3g (1/2, 0, 1/2) sites. Five nonequivalent interstices have been reported to be available to the hydrogen. Their positions are given in Table 1, together with their neighbouring metal atom coordinates and their hole radii [18]. The hole radius is defined by the maximum radius of a sphere which touches the surfaces of the neighbouring metal atom spheres without overlapping. No interstitial spheres are required for the LMTO-ASA calculations for $LaNi_5$.

For the hydrogen solutions (the α-phase), no ordered structures with full site occupancy have been reported; the hydrogen atoms only partially occupy the available hydrogen sites and the crystal symmetry remains the same as that of the host alloy ($P6/mmm$) [18,19]. In this work, we employed hypothetical unit cells by doubling the unit cell of $LaNi_5$ along the c-axis and putting one hydrogen atom at one of the possible sites, namely $La_2Ni_{10}H$, in order to see the relative stability of the solid solutions. For $La_2Ni_{10}H$, interstitial spheres have to be included in order to pack the whole volume of the lattice.

For the full hydride (the β-phase), two ordered structures have been reported [20] based on a careful interpretation of the neutron diffraction data. (We should note, however, that the structures with the same crystal symmetry as $LaNi_5$ but with fractional site occupancies of the hydrogen atoms have also been reported [21]). The ordered structures have the $P6_3mc$ and the $P31c$ symmetries respectively, both of which have a doubled unit cell of $LaNi_5$ along the c-axis and contain 14 hydrogen atoms at three different hydrogen sites, namely $La_2Ni_{10}H_{14}$. Structural data for $La_2Ni_{10}H_{14}$ are given in Table 2 for each symmetry. These structures are both slightly distorted from the original symmetry of $LaNi_5$ ($P6/mmm$). The authors of Ref. [20] were not able to judge from their experimental data which symmetry is more probable, $P6_3mc$ or $P31c$. We will show later that the structure with the $P6_3mc$ symmetry is more probable in terms of the calculated total energy.

The crystal structure with the $P6_3mc$ symmetry is shown in Fig. 2. In this structure. there are three nonequivalent hydrogen sites, 2b, 6c1 and 6c2. A list of nearest neighbour atoms of the three hydrogen atoms up to the first nearest hydrogen atoms is given in Table 3. These ordered structures allow us to calculate the electronic structure for the hydride within a relatively small unit cell. Interstitial spheres are required to fill the whole volume for both structures.

All lattice parameters were taken from the experimentally determined values: $a=9.481$ and $c=7.532$ for $LaNi_5$ [22], $a=9.495$ and $c=15.082$ for $La_2Ni_{10}H$ [18] and $a=10.221$ and $c=16.252$ for $La_2Ni_{10}H_{14}$ [20] (all in atomic unit). The lattice expands considerably by 23.4% after the hydrogen absorption to the full hydride [20]. For the full hydride, the minimum distance between the hydrogen and the nickel is 2.94 a.u.(H1–Ni1), and that between the hydrogen atoms is 4.90 a.u.(H2–H2). The minimum distances between the metal atoms are 8.13 a.u.(La–La), 5.90 a.u.(La–Ni1) and 4.87 a.u.(Ni2–Ni3), respectively.

3. Results and discussion

3.1. Calculational parameters

3.1.1. Overlap conditions

As mentioned in Section 2.1, the interstitial spheres have to be included in order to fill the whole volume of an

Table 1
Interstitial sites in the unit cell of $LaNi_5$ [18]

Site	x	y	z	Coordination	Hole radius (a.u.)
3f	0.5	0	0	La×2, Ni1×2, Ni2×2	0.486
4h	0.333	0.667	0.37	Ni1×1, Ni2×3	0.569
6m	0.137	0.274	0.5	La×2, Ni2×2	1.042
12o	0.204	0.408	0.354	La×1, Ni1×1, Ni2×2	0.733
12n	0.455	0.0	0.117	La×1, Ni1×2, Ni2×1	0.771

Table 2
Structural data for $La_2Ni_{10}H_{14}$ with the $P6_3mc$ and $P31c$ symmetries [18]

$La_2Ni_{10}H_{14}$		$a=10.221$ a.u.		$c=16.252$ a.u.			
Space group	Pearson symb.	Atom	Wyckoff symb.	Symmetry	x	y	z
$P6_3mc$	hP26	La	2a	3m.	0	0	0.9999
		H1	2b	3m.	1/3	2/3	0.8203
		Ni1	2b	3m.	1/3	2/3	0.0011
		Ni2	2b	3m.	1/3	2/3	0.4881
		H2	6c	.m.	0.1593	0.8407	0.2952
		H3	6c	.m.	0.5069	0.4931	0.0577
		Ni3	6c	.m.	0.4999	0.5001	0.2500
$P31c$	hP26	La	2a	3..	0	0	0.0037
		H1	2b	3..	1/3	2/3	0.8297
		Ni1	2b	3..	1/3	2/3	0.0061
		Ni2	2b	3..	1/3	2/3	0.4968
		H2	6c	1	0.1680	0.3223	0.2993
		H3	6c	1	0.4895	0.9994	0.0574
		Ni3	6c	1	0.4859	0.0028	0.2500

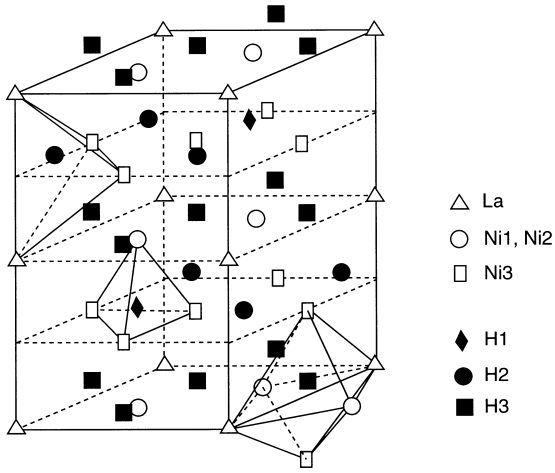

Fig. 2. Crystal structure of $La_2Ni_{10}H_{14}$ ($P6_3mc$).

Table 3
Nearest neighbour atoms of the nonequivalent hydrogen atoms in $La_2Ni_{10}H_{14}$ with the $P6_3mc$ symmetry [18]

Centre	1	2	3	4	5	6	7	8
H1	Ni1	Ni3	H3	H2	H2			
	1	3	3	3	6			
	2.94	3.17	4.93	5.12	5.13			
	1.00	1.08	1.68	1.74	1.75			
H2	Ni3	La	Ni2	H2	H3	H1	H3	H2
	2	1	1	3	2	2	2	2
	3.11	4.36	4.40	4.88	4.94	5.13	5.19	5.34
	1.00	1.40	1.42	1.57	1.59	1.65	1.67	1.72
H3	Ni2	Ni3	Nil	H3	H1	H2		
	1	1	1	2	1	2		
	3.05	3.13	3.21	4.90	4.93	4.94		
	1.00	1.03	1.05	1.61	1.62	1.62		

upper: atom i
middle upper: number of atoms, N_i
middle lower: distance, d_i (a.u.)
lower: normalised distance, d_i/d_1

open-structured material. This is the case for the hydrogen solutions and the hydride, while no interstitial spheres are required for the host alloy $LaNi_5$. The number and size of the interstitial spheres will vary for different overlap conditions. Thus, we first calculated the total energy of $La_2Ni_{10}H_{14}$ for different overlap conditions in order to check their influence. The results are summarised in Table 4. As can be seen from this table, the total energy per formula unit varies by much as 0.3 Ry as the relative sphere overlap factor $\omega_{\mathbf{RR}'}$ changes from 21.7 to 17.7%. This result demonstrates that the total energy is sensitive to the shape of the potential wells and ultimately to the choice of basis functions in the interstitial regions. It suggests that the total energy calculations would be improved considerably by using full-potential methods like the full-potential LMTO technique which can describe the interstitial potential accurately [10,11]. The minimum total energy was obtained for the condition that the number of interstitial spheres is equal to 58, which we used for all subsequent calculations.

3.1.2. Kinetic energy of the electron in the interstitial regions

In the LMTO formalism, the kinetic energy of an electron in the interstitial regions κ^2 can be treated as an independent parameter. This parameter, which determines

Table 4
Influence of the overlap conditions on the total energy of $La_2Ni_{10}H_{14}$

$\omega_{\mathbf{RR}'}$ (%)			N^{IS}	r^{IS}_{min}	U^{tot}
AT-AT	AT-IS	IS-IS	(-)	(a.u.)	(Ry f.u.$^{-1}$)
17.1	21.7	23.1	42	1.046	−64373.8284
17.4	18.5	20.5	58	0.898	−64374.1184
16.0	17.7	19.7	68	0.816	−64374.0228

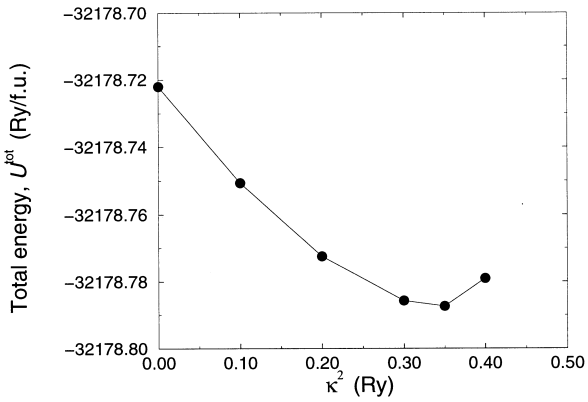

Fig. 3. Total energy per formula unit of $LaNi_5$ vs κ^2.

the long-range behaviour of the muffin-tin orbitals, affects the total energy within the ASA. In Figs. 3 and 4 the total energy curves as a function of κ^2 for $LaNi_5$ and $La_2Ni_{10}H_{14}$, respectively are shown. In each case the total energy reaches a minimum at $\kappa^2=0.35$ Ry and the difference in the total energy per atom between, $\kappa^2=0$ and $\kappa^2=0.35$ Ry is approximately 10 mRy. This result shows that the theoretical value of the total energy is lowered by 10 mRy per atom by optimising the parameter κ^2 or the shape of the muffin-tin orbitals. For the following calculations we set $\kappa^2=0.35$ Ry.

3.1.3. Spin polarization

For materials with a large magnetic moment, the total energy calculated with the spin-polarised LDA may differ considerably from that calculated with the non-spin-polarised LDA. In order to see the influence of the spin-polarization, we calculated the total energy of $LaNi_5$ and

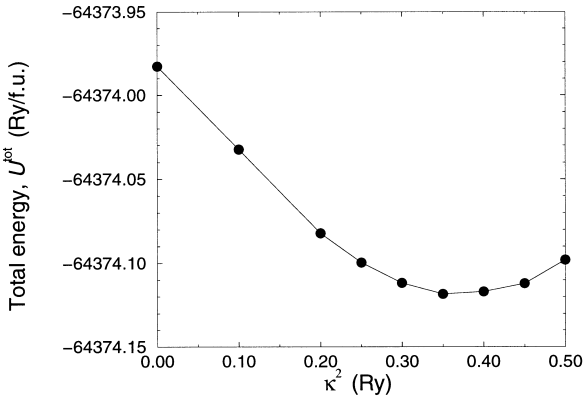

Fig. 4. Total energy per formula unit of $La_2Ni_{10}H_{14}$ vs κ^2.

Table 6
Influence of number of the **k**-point on the total energy of $La_2Ni_{10}H_{14}$

$(n_{k_x}, n_{k_y}, n_{k_z})$	$n_{\mathbf{k}}^{irr}$	$n_{\mathbf{k}}^{tot}$	U^{tot} (Ry f.u.$^{-1}$)
(6, 6, 2)	14	72	−64374.0973
(6, 6, 6)	42	216	−64374.0976
(11, 11, 11)	96	1331	−64374.0970

$La_2Ni_{10}H_{14}$ with each of the methods. The total energy and magnetic moment of $LaNi_5$ and $La_2Ni_{10}H_{14}$ are shown in Table 5. The magnetic moment of $LaNi_5$ is predicted to be 0.602 μ_B per formula unit (μ_B is the Bohr magneton), which is almost the same as that calculated previously with the augmented plane wave (APW) method [23]. Therefore, the magnetic moment per nickel atom is one-sixth that of fcc-Ni [24]. The magnetic moment of $La_2Ni_{10}H_{14}$ is predicted to be zero. The difference in the total energy is less than the order of 1 mRy per formula unit (0.02 mRy for $LaNi_5$ and 0.26 mRy for $La_2Ni_{10}H_{14}$). These results justify the use of non-spin-polarised calculations in order to obtain the theoretical heat of formation of the $LaNi_5$ hydride.

3.1.4. Number of **k**-points

The total energies of $La_2Ni_{10}H_{14}$ for different numbers of **k**-points, $(n_{k_x}, n_{k_y}, n_{k_z})=(6, 6, 2)$, (6, 6, 6) and (11, 11, 11)), are shown in Table 6 together with the number of irreducible **k**-points and the total number of **k**-points. We see that the total energies remain almost unchanged; they vary by only the order of 10^{-1} mRy per formula unit. Thus we set the number of **k**-points as $(n_{k_x}, n_{k_y}, n_{k_z})=(6, 6, 2)$ for the following calculations in order to reduce the memory and time for computation.

3.2. $LaNi_5$

The energy band structure and the total and partial densities of states (DOSs) of $LaNi_5$ are shown in Figs. 5 and 6 respectively, where the Fermi energy E_F has been taken as the energy zero. The states below E_F consist mainly of the Ni 3d band. As expected, the Fermi energy falls near the top of the Ni d band with the contribution from La states being almost zero. These LMTO-ASA densities of states are similar to those calculated previously by the APW method [23] and by the TB-recursion method [25]. We have also calculated the valence charge density, which is shown in Fig. 7 for the $(2\bar{1}\bar{1}0)$ plane along the *c*-axis. It clearly illustrates the high charge density regions

Table 5
Influence of the spin-polarization on the total energy

M (MH)	U_{LDA}^{tot} (Ry f.u.$^{-1}$)	U_{LSD}^{tot} (Ry f.u.$^{-1}$)	Magnetic moment (μ_B f.u.$^{-1}$)
$LaNi_5$	−32178.7873	−32178.7873	0.602
$La_2Ni_{10}H_{14}$	−64374.1182	−64374.1184	0.000

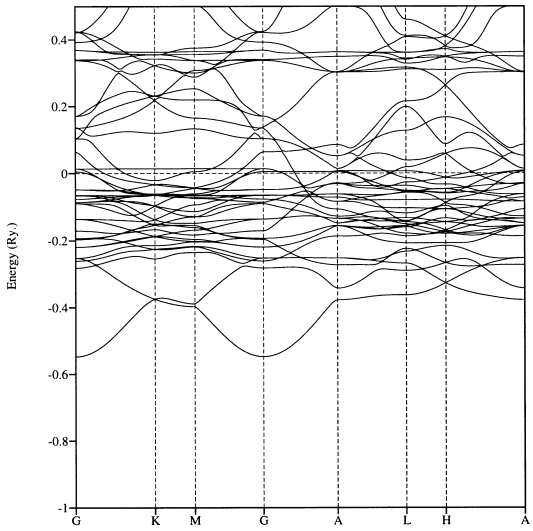

Fig. 5. Energy band structure of $LaNi_5$. (G denotes Γ.)

centred at the Ni atoms and the low charge density interstitial regions. The bond charge between the Ni1 and the Ni2 atoms can also be seen in this figure.

As shown in Table 1, there are five possible interstitial sites available for hydrogen. We have calculated the charge densities at the different interstitial sites, since these are considered to be related to the preferred site occupation by hydrogen [26–28]. The results are summarised in Table 7 together with the hole radii of the sites [18] and the site occupancies determined by neutron diffractometry for the hydrogen solutions [18,19] and the full hydride [21] with the *P*6/*mmm* symmetry. (Note that for the hydrogen solutions the 3f and 12n hydrogen sites have been reported by neutron diffractometry, while the coexistence of the 3f and 6m hydrogen sites have also been demonstrated by an inelastic neutron scattering study [29].) According to effective medium theory [26–28] the binding energy of a hydrogen atom in a homogeneous electron gas is described

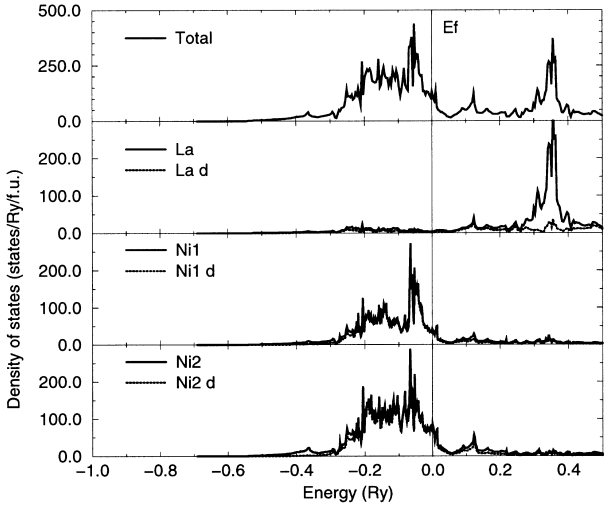

Fig. 6. Density of states of $LaNi_5$.

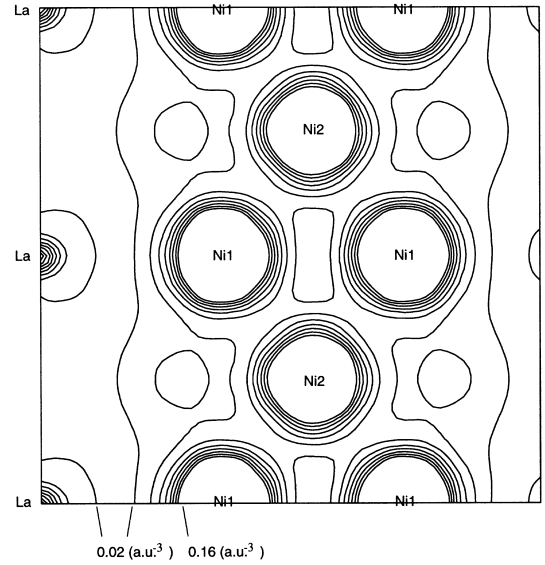

Fig. 7. Valence electron density of $LaNi_5$ for the $(2\bar{1}\bar{1}0)$ plane. (Mapping area 2c×2c, inner-most contour 0.16 a.u.$^{-3}$, outer-most 0.02 a.u.$^{-3}$, 0.02 a.u.$^{-3}$ step.)

by a unique function of the electron density, which displays an energy minimum at the electron density of 0.002 a.u.$^{-3}$. Since the electron densities at the interstitial sites in $LaNi_5$ are at least an order of magnitude greater than this, the interstitial sites with the greatest binding energy will have the least electron density. From Table 8 we see that this corresponds to the 6m site, in good agreement with the experimentally determined site occupancies for the hydride since this corresponds to the site with biggest occupancy of hydrogen [21]. For the rest of the interstitial sites for the hydride and those for the hydrogen solutions, however, the charge density does not correlate either with the site occupancy or with the hole size, which suggests that a more careful treatment beyond effective medium theory is required to explain the observed site occupation by hydrogen.

3.3. α-$La_2Ni_{10}H$

The energy band structure and the total and partial densities of states of $La_2Ni_{10}H$ with the hydrogen atom at

Table 7
Electron densities at the possible hydrogen sites in $LaNi_5$

H site	Hole radius (a.u.)	n_e (a.u.$^{-3}$)	α-phase[a]	Occupancy α-phase[b]	β-phase[c]
3f	0.486	0.0315	–	0.07	0.21
4h	0.569	0.0368	–	–	0.13
6m	1.042	0.0234	–	–	0.32
12n	0.771	0.0308	0.04	–	0.18
12o	0.639	0.0318	–	–	0.11

[a] Ref. [18]; composition $La_2Ni_{10}H_{0.8}$.
[b] Ref. [19]; composition $La_5Ni_{25}H_{0.9}$.
[c] Ref. [21]; composition $La_{1.95}Ni_{10}H_{13}$.

Table 8
Total energy per formula unit and heat of solution of $La_2Ni_{10}H$ for the different hydrogen sites

H site	$\omega_{RR'}$ (%)			N^{IS}	U^{tot}	ΔH
	AT-AT	AT-IS	IS-IS	(-)	(Ry f.u.$^{-1}$)	(kJ mol^{-1} H_2)
3f	13.7	-	-	0	−64358.2125	1378.5
4h	16.0	18.0	20.0	27	−64358.3683	967.3
6m	16.0	16.2	14.2	10	−64358.3973	890.8
12n	16.0	18.0	12.4	12	−64358.1936	1428.4
12o	16.0	16.5	17.7	15	−64358.1386	1573.7

the 6m site are shown in Figs. 8 and 9, respectively. As is clearly seen in Fig. 8, one lower energy state has appeared after the hydrogen absorption, which has been formed with the hybridization between the hydrogen s orbitals and the nickel spd orbitals. The Fermi energy has shifted to a higher energy level by 0.043 Ry compared with that of $LaNi_5$, while the relative position of the Fermi energy remains unchanged and falls at the edge of the nickel d bands. There is a gap of width of 0.1 Ry between the lower energy states and the rest of the bands.

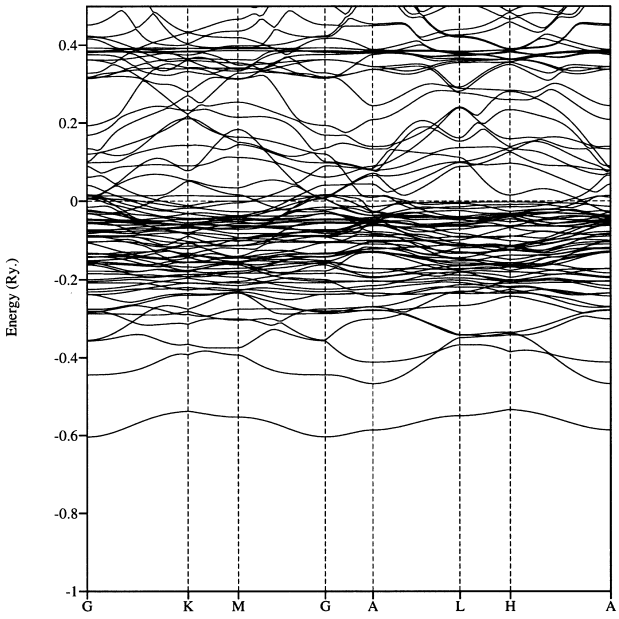

Fig. 8. Energy band structure of $La_2Ni_{10}H$ (H; 6m site).

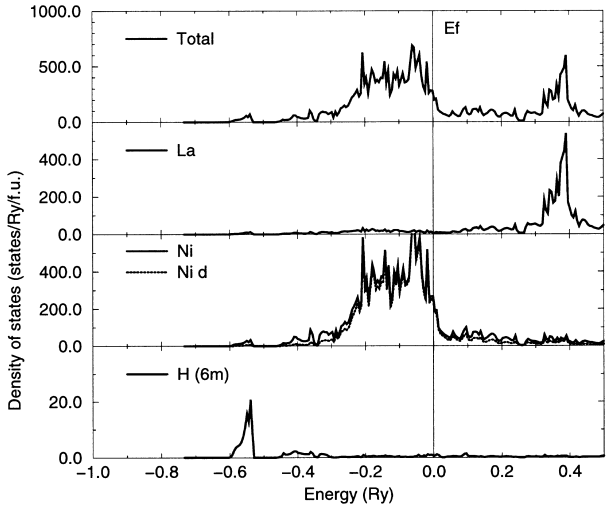

Fig. 9. Density of states of $La_2Ni_{10}H$ (H; 6m site).

The total energies of $La_2Ni_{10}H$ for the different hydrogen sites are shown in Table 8. The predicted relative stability is 6m<4h<3f<12n<12o. This order shows again that the 6m site is the most stable. However, the rest of the order does not correlate either with the charge density or with the experimentally determined site occupancy. One reason for this disagreement could be due to the difference in the number of interstitial spheres contained in the unit cells, which could lead to differences in the total energy of the order of 0.1 Ry per formula unit as described in Section 3.1.1.

We have also calculated the heat of formation of $La_2Ni_{10}H$ (the heat of hydrogen solution) from the total energy calculated for each structure. The results are given in Table 8. All the values of the heat of solution turned out to be positive and unrealistically large compared with the experimental value of -59 kJ mol^{-1} H_2 [30], even for the most stable structure (0.337 Ry f.u.$^{-1}$ = 890 kJ mol^{-1} H_2). This unfavourable result clearly indicates that local relaxation of the metal atoms surrounding the hydrogen atoms must be considered in order to predict the heat of solution correctly, although it cannot be detected by diffractometry. The order of the relative stability might be affected by this local relaxation and will be considered during future work.

In Fig. 10, summarising the results of Sections 3.2 and 3.3, the preferred site occupancy with the hole radius, the inverse cube root of the electron density, and the heat of solution between the possible hydrogen sites in the *P*6/*mmm* structure are compared. All the results show roughly the same trend except for the 4h heat of solution. All indicate that 6m site is the most preferred as already mentioned.

3.4. β-$La_2Ni_{10}H_{14}$

First, we calculated the total energies of $La_2Ni_{10}H_{14}$ for the two different structures. namely $P6_3mc$ and $P31c$ (Table 2), in order to see which structure is more probable. The results are shown in Table 9. For the same number of

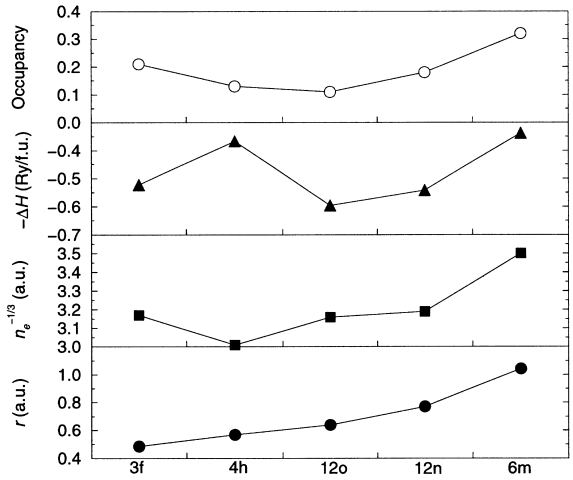

Fig. 10. Comparison between the hole radius, the inverse cube root of the electron density, the heat of solution and the experimental site occupancy for the hydride.

the interstitial spheres, the $P6_3mc$ structure exhibits a lower total energy by 0.0871 Ry f.u.$^{-1}$ This indicates that the $P6_3mc$ structure is more probable, which could not be confirmed by the neutron diffraction data [20]. We thus employ the $P6_3mc$ structure for $La_2Ni_{10}H_{14}$ for the following calculations.

The energy band structure and the total and partial densities of states of $La_2Ni_{10}H_{14}$ are shown in Figs. 11 and 12, respectively. (The partial density of states of the interstitial spheres is not shown.) The lower energy states are formed by the hybridization of the s orbitals of the absorbed hydrogen with the lower energy portion of the $LaNi_5$ states, mainly with the Ni orbitals and partly with the La orbitals. Similarly to $La_2Ni_{10}H$, a gap of 0.1 Ry is observed between these lower energy states and the rest of the band, the majority of which is the Ni d band. The lower energy states are essentially hydrogen-derived states; the integrated number of the electrons up to the gap is 28 as is confirmed by the energy band structure in Fig. 11. The relative position of the Fermi energy hardly changes from that for $LaNi_5$ it falls at the top of the Ni d band and the contribution of La remains almost zero at the Fermi energy. This picture is different from that predicted by the TB recursion method [25], where the contributions at the Fermi energy from the Ni atoms and the La atoms have been reported to be comparable. Looking into the hydrogen derived states, they are separated into two parts by a small gap of approximately 0.03 Ry. This small gap can

Table 9
Comparison between the total energies of $La_2Ni_{10}H_{14}$ with different crystal symmetry

Symmetry	$\omega_{RR'}$ (%)			N^{IS}	U^{tot}
	AT-AT	AT-IS	IS-IS	(-)	(Ry f.u.$^{-1}$)
$P6_3mc$	17.1	21.7	23.1	42	−64374.0228
$P31c$	16.8	18.6	18.6	42	−64373.9357

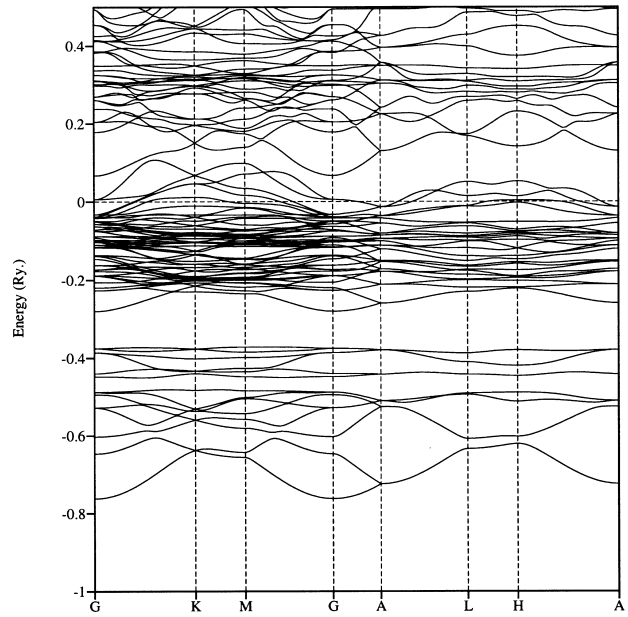

Fig. 11. Energy band structure of $La_2Ni_{10}H_{14}$.

not be seen in the DOS calculated with the TB recursion method. The lower energy states consist mainly of the H3 states and the higher states mainly of the H2 states. The H1 states extend evenly throughout both regions. The integrated number of the electrons in the interstitial spheres up to the Fermi energy is relatively small; it is 12.7, about one-tenth of the total number of the valence electrons (120 electrons). These electrons, which come from both the metal atoms and the hydrogen atoms, would not affect the general description of the nature of the densities of states.

The valence electron density of $La_2Ni_{10}H_{14}$ for the $(2\bar{1}10)$ plane along the *c*-axis is shown in Fig. 13. The centres of the H1, H2 and H3 hydrogen atoms all lie in this plane. Bond charges between the hydrogen atoms and the nickel atoms are clearly seen. (Those between H2 and Ni3

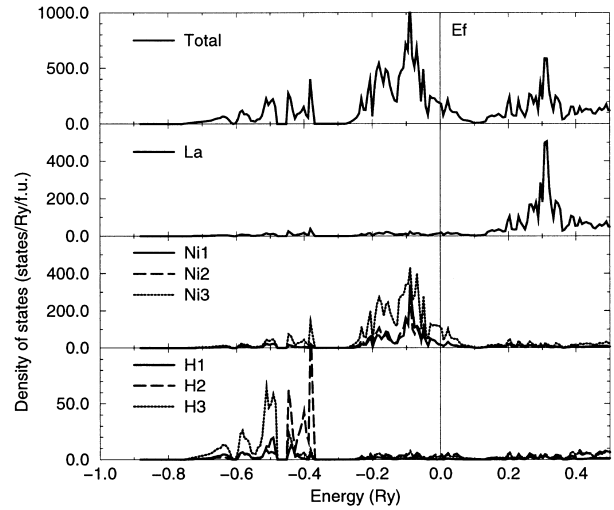

Fig. 12. Density of states of $La_2Ni_{10}H_{14}$.

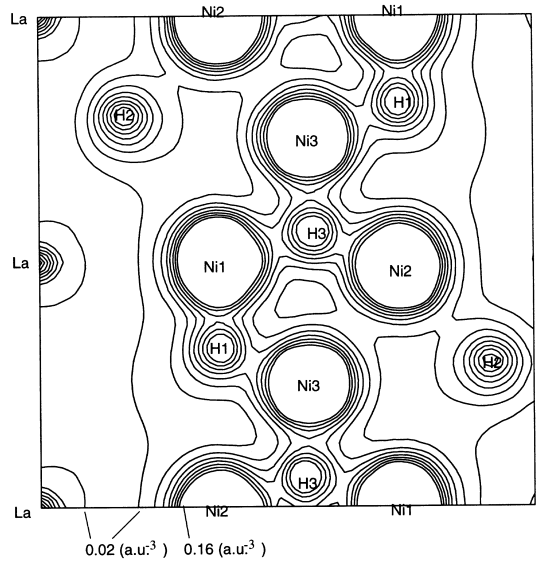

Fig. 13. Valence electron density of $La_2Ni_{10}H_{14}$ for the $(2\bar{1}\bar{1}0)$ plane. (Mapping area 2c×2c, inner-most contour 0.16 a.u.$^{-3}$, outer-most 0.02 a.u.$^{-3}$, 0.02 a.u.$^{-3}$ step.)

are not in this plane.) On the other hand, no clear bond charges between the hydrogen atoms and the lanthanum atoms can be seen in this figure; the interaction between the lanthanum and the hydrogen would be more ionic than covalent because of the large electronegativity difference between lanthanum and hydrogen.

Finally, we have calculated the theoretical heat of formation of the hydride from the total energies of $LaNi_5$, $La_2Ni_{10}H_{14}$ and H_2. As can be seen from the density of states in Fig. 12, the hydrogen absorption causes a large change in the electronic structure of the host metal. This is accompanied by a slight symmetry distortion from *P*6/*mmm* to $P6_3mc$ and a lattice expansion of 25%. In order to investigate which contribution is dominant for the heat of formation, we have calculated the total energies U_M^{dist} and U_M^{relax} of two hypothetical structures: an internally *distorted* structure without hydrogen, namely La_2Ni_{10}, with the same symmetry as the hydride ($P6_3mc$) but with the equilibrium volume of La_2Ni_{10}, and an *expanded* La_2Ni_{10} with the $P6_3mc$ structure, but with the same equilibrium volume as $La_2Ni_{10}H_{14}$. Here we kept the same overlap conditions in order to minimise their influence on the energy differences. For the distorted La_2Ni_{10} and the expanded La_2Ni_{10}, we replaced the fourteen hydrogen atoms of $La_2Ni_{10}H_{14}$ with the $P6_3mc$ structure with the same number of the interstitial spheres; thus the total number of the interstitial spheres is 58+14=72. The calculated total energies are summarised in Table 10. The theoretical heat of formation per molecular hydrogen ΔH for the hydrogenation reaction,

$$\tfrac{2}{7}\ LaNi_5 + H_2 = \tfrac{1}{7}\ La_2Ni_{10}H_{14} + \Delta H, \quad (6)$$

was calculated as follows:

$$\Delta H = \tfrac{1}{7}\{U_{MH} - 2U_M - 7U_{H_2}\}$$

$$= \tfrac{1}{7}\{(U_{MH} - U_M^{exp} - 7U_{H_2}) + (U_M^{exp} - U_M^{dist}) + (U_M^{dist} - 2U_M)\}$$

$$= \tfrac{1}{7}\{(-0.7292) + (0.3110) + (0.1144)\}$$

$$= -0.0434\ \text{Ry mol}^{-1}\ H_2$$

$$= -57.3\ \text{kJ mol}^{-1}\ H_2, \quad (7)$$

where U_{MH}, U_M^{exp}, U_M^{dist}, U_M, U_{H_2} are the total energies of $P6_3mc$ $La_2Ni_{10}H_{14}$ at its equilibrium volume, $P6_3mc$ La_2Ni_{10} expanded to the equilibrium volume of $La_2Ni_{10}H_{14}$, La_2Ni_{10} with distortion to the $P6_3mc$ symmetry at the equilibrium volume of $LaNi_5$, the host alloy $LaNi_5$ at its equilibrium volume and the hydrogen molecule, respectively. In the second line of Eq. (7), the first, second and third terms represent contributions from the change in the electronic structure (due to chemical bonding), volume relaxation (due to size effects), and the change in the crystal symmetry from *P*6/*mmm* to $P6_3mc$ (due to internal distortion), respectively. Here we obtained a negative heat of formation of -57.3 kJ mol^{-1} H_2. The main contribution to the negative heat of formation has been found to come from the change in the electronic structure. This large negative contribution compensates the positive contributions both from the volume expansion and from the change in the crystal symmetry, which reflect an energy cost for the deformation of the lattice as normally expected. The contribution from the change in the crystal symmetry is relatively small. It is worth stressing that the heat of formation is determined by a subtle balance between these contributions, its absolute value being much smaller than each individual contribution. In this case, even the theoretical total energy of the hydrogen molecule

Table 10
Total energies used for calculation of the heat of formation of $La_2Ni_{10}H_{14}$

M	Symmetry	*a* (a.u.)	*c* (a.u.)	N^{IS}	U^{tot} (Ry f.u.$^{-1}$)
$La_2Ni_{10}H_{14}$	$P6_3mc$	10.221	16.252	58	−64374.1184
La_2Ni_{10} (expanded)	$P6_3mc$	10.221	16.252	58+14	−64357.1492
La_2Ni_{10} (distorted)	$P6_3mc$	9.481	15.064	58+14	−64357.4602
$LaNi_5$	*P*6/*mmm*	9.481	7.532	0	−32178.7873
H_2 (LSD)[a]	–	–	–	–	−2.320

[a] Ref. [16].

can be decisive; if the value calculated with the Hartree–Fock approximation is used instead of that calculated with the local spin density approximation (LSD) [16], then the heat of formation would become more negative by 70 kJ mol^{-1} H_2.

Although the calculated heat of formation is negative, it is overestimated by almost a factor of two compared with the experimental heat of formation (-30 kJ mol^{-1} H_2 [30–32]). From the viewpoint of the computational design of alloys with suitable equilibrium hydrogen pressures, the theoretical value of -57.3 kJ mol^{-1} H_2 is very unfavourable as the difference between the theoretical value and the experimental one corresponds to almost five orders in the equilibrium hydrogen pressure assuming a constant entropy change in Eq. (5). Two factors may be responsible for this error in the heat of formation and also the heat of solution: one is the internal relaxation of the atoms, which we did not take into account, and the other is the unsatisfactory representation of the potentials in the interstitial regions by the interstitial spheres. The value of the theoretical heat of formation is expected to be improved by using full-potential methods such as the full-potential LMTO method [10,33,34].

4. Conclusions

In this paper, we have investigated the electronic structure and energetics of $LaNi_5$ and its hydrogen solutions (the α-phase) and hydride (the β-phase) by using the TB-LMTO-ASA method. After optimising the calculational parameters, we obtained the following results:

- The 6m site in the $P6/mmm$ structure has been found to be the most easily available for the hydrogen atoms in terms of both the charge density of the host alloy and the heat of formation of the hydrogen solutions. The heats of solution turned out to be unrealistically large and positive, which clearly indicates that local relaxation around the hydrogen atoms must be considered in order to obtain the correct value.
- Two split-off hydrogen-derived bands have been predicted, which arise mainly from the bonding between the hydrogen s orbitals and the nickel spd orbitals. The small gap between these two split-off bands was not seen in the DOS calculated by the TB-recursion method [25].
- We successfully obtained the negative heat of formation from the total energy calculations, although it is still overestimated compared with experiment. The main contribution to the negative heat of formation has been found to arise from the change in the electronic structure (chemical bonding), which compensates the positive contributions from the volume expansion (size effect) and the internal distortion.

The predicted value of the heat of formation is expected to be improved by using full-potential methods such as the full-potential LMTO method, which is our future task. We are also planning to study the details of the bonding energy between the atoms by using the two-centre TB Hamiltonian described in Section 2.1.

Acknowledgements

HN is grateful for financial support from SANYO Electric Co. DNM would like to thank Dr. O. Gunnarsson for providing his result for the total energy of the hydrogen molecule and Prof. O.K. Andersen for useful discussions on the LMTO method. Computations were performed in the Materials Modelling Laboratory, Department of Materials, University of Oxford.

References

[1] J.H.N. van Vucht, F.A. Kuijpers, H.C.A.M. Bruning, Philips Res. Rep. (1970) 133.
[2] H.H. van Mal, K.H.J. Buschow, A.R. Miedema, J. Less-Common Met. 35 (1974) 65.
[3] A. Percheron-Guégan, C. Lartigue, J.C. Archard, J. Less-Common Met. 109 (1985) 287.
[4] H. Nakamura, Y. Nakamura, S. Fujitani. I. Yonezu. J. Alloys Comp. 252 (1997) 83.
[5] G. Krier, O. Jepsen, A. Burkhart, O.K. Andersen, The TB-LMTO-ASA programme, Stuttgart, 1995.
[6] U. von Barth, L. Hedin, J. Phys. C 5 (1972) 1629.
[7] D.C. Langreth, M.J. Mehl, Phys. Rev. B 28 (1983) 1809.
[8] C.D. Hu, D.C. Langreth, Phys. Rev. B 33 (1986) 943.
[9] O.K. Andersen, et al., Mater. Res. Symp. Proc. 253 (1992) 37.
[10] M. Methfessel, Phys. Rev. B 38 (1988) 1537.
[11] O.K. Andersen, O. Jepsen, G. Krier, in: V. Kumar, O.K. Andersen, A. Mookerjee (Eds.), Method of Electronic Structure Calculations, Worth Scientific, 1994, p. 1.
[12] O.K. Andersen, O. Jepsen, D. Glötzel, in: F. Bassani, F. Fumi, M.P. Tosi (Eds.), Highlight of Condensed-Matter Theory, North-Holland, New York, 1985, p. 1.
[13] O.K. Andersen, Z. Powlowska, O. Jepsen, Phys. Rev. B 34 (1986) 5253.
[14] O. Jepsen, O.K. Andersen, Z. Phys. B 97 (1995) 35.
[15] P. Blochl, O.K. Andersen, O. Jepsen, Phys. Rev. B 49 (1994) 16223.
[16] O. Gunnarsson, private communication. Only binding energy of the hydrogen molecule is given in O. Gunnarsson, Int. J. Quantum Chem. 10 (1976) 307.
[17] D. Ohlendorf, H.E. Flotow, J. Chem. Phys. 73 (1980) 2937.
[18] J.L. Soubeyroux, A. Percheron-Guégan, J.C. Achard, J. Less-Common Met. 129 (1987) 181.
[19] P. Fischer, A. Furrer, G. Busch, L. Schlapbach, Helv. Phys. Acta 50 (1977) 421.
[20] C. Lartigue, A. Le Bail, A. Percheron-Guégan, J. Less-Common Met. 129 (1987) 65.
[21] A. Percheron-Guégan, C. Lartigue, J.C. Achard, P. Germi, F. Tasset, J. Less-Common Met. 74 (1980) 1.
[22] A. Furrer, P. Fischer, W. Hälg, L. Schlapbach, Hydrides for energy storage, Proceedings of an International Symposium, Norway 1977 (1978) 73.

[23] S.K. Malik, F.J. Arlinghaus, W.E. Wallace, Phys. Rev. B 25 (1982) 6488.
[24] H. Nakamura, unpublished data.
[25] M. Gupta, J. Less-Common Met. 130 (1987) 219.
[26] M.J. Puska, R.M. Nieminen, M. Manninen, Phys. Rev. B 24 (1981) 3037.
[27] J.K. Nørskov, Phys. Rev. B 26 (1982) 2875.
[28] J.K. Nørskov, F. Besenbacher, J. Less-Common Met. 130 (1987) 475.
[29] R. Hempelmann, D. Richter, G. Eckold, J.J. Rush, J.M. Rowe, M. Montoya, J. Less Common Met. 104 (1984) 1.
[30] J.J. Murray, M.L. Post, J.B. Taylor, J. Less-Common Met. 80 (1981) 211.
[31] B.S. Bowerman, C.A. Wulff, T.B. Flanagan, Z. Phys. Chem. 116 (1979) 197.
[32] W.N. Hubbard, P.L. Rawlins, P.A. Connick, R.E. Stedwell, P.A.G. O'Hare, J. Chem. Thermo. 13 (1983) 785.
[33] D. Nguyen-Manh, A. Pasturel, A.T. Paxton, M. van Schilfgaarde, Phys. Rev. B 48 (1993) 14801.
[34] A. Neumann, D. Nguyen-Manh, A. Kjekshus, A.P. Sutton, Phys. Rev. B 57 (1998) 11149.